



Numerical modeling of self-pressurization and pressure control by a thermodynamic vent system in a cryogenic tank



Alok Majumdar^{a,*}, Juan Valenzuela^a, Andre LeClair^a, Jeff Moder^b

^a NASA Marshall Space Flight Center, Huntsville, AL 35812, USA

^b NASA Glenn Research Center, 21000 Brookpark Road, Cleveland, OH 44135, USA

ARTICLE INFO

Article history:

Received 25 June 2015

Received in revised form 23 November 2015

Accepted 1 December 2015

Available online 15 December 2015

Keywords:

Cryogenic fluid management

Numerical model

ABSTRACT

This paper presents a numerical model of a system-level test bed—the multipurpose hydrogen test bed (MHTB) using the Generalized Fluid System Simulation Program (GFSSP). MHTB is representative in size and shape of a space transportation vehicle liquid hydrogen propellant tank, and ground-based testing was performed at NASA Marshall Space Flight Center (MSFC) to generate data for cryogenic storage. GFSSP is a finite volume-based network flow analysis software developed at MSFC and used for thermofluid analysis of propulsion systems. GFSSP has been used to model the self-pressurization and ullage pressure control by the Thermodynamic Vent System (TVS). A TVS typically includes a Joule–Thompson (J–T) expansion device, a two-phase heat exchanger (HEX), and a mixing pump and liquid injector to extract thermal energy from the tank without significant loss of liquid propellant. For the MHTB tank, the HEX and liquid injector are combined into a vertical spray bar assembly. Two GFSSP models (Self-Pressurization and TVS) were separately developed and tested and then integrated to simulate the entire system. The Self-Pressurization model consists of multiple ullage nodes, a propellant node, and solid nodes; it computes the heat transfer through multilayer insulation blankets and calculates heat and mass transfer between the ullage and liquid propellant and the ullage and tank wall. A TVS model calculates the flow through a J–T valve, HEX, and spray and vent systems. Two models are integrated by exchanging data through User Subroutines of both models. Results of the integrated models have been compared with MHTB test data at a 50% fill level. Satisfactory comparison was observed between tests and numerical predictions.

Published by Elsevier Ltd.

1. Introduction

Numerical modeling of Cryogenic Fluid Management (CFM) applications such as long-term storage of cryogen in space is very important to meet technological challenges of future missions. Numerical modeling tools need to have the sufficient fidelity to answer critical design and operational issues and must be verified by comparing with test data. The purpose of this paper is to develop a system-level model of self-pressurization of a cryogenic tank with multiple nodes and verify the numerical predictions by comparing with test data. The test data from the multipurpose hydrogen test bed (MHTB) [1] was used to verify the numerical model developed with the Generalized Fluid System Simulation Program (GFSSP) [2].

MHTB (Fig. 1) is also capable of accommodating various CFM concepts and research. The aluminum (Al) 5083 tank is cylindrical

shaped with a diameter of 10 feet, a height of 10 feet, and 2:1 elliptical domes. Its size is comparable to a full-scale cryogenic tank. The tank is enclosed in Al shroud for uniform and controllable temperature distribution throughout the outer surface of the passive insulation system. The entire test article is placed inside a 20-ft-diameter vacuum chamber to simulate deep space thermal conditions.

The passive thermal control system of the MHTB is comprised of a combination of spray-on foam insulation (SOFI) and a multilayer insulation (MLI) system. The SOFI is a robotically sprayed-on application similar to that used in the Space Shuttle external tank foam application process. It has a nominal thickness of 0.56 inch throughout the surface area of the tank. The MLI is comprised of a 45-layer variable density blanket placed over the SOFI. The blanket is composed of 0.5 mil double-aluminized Mylar as the radiation shield with B4A Dacron netting as the spacer layer between the Mylar. B4A Dacron bumper strips are used to create the variable density effect where there are fewer layers of MLI closer to

* Corresponding author.

E-mail address: alok.k.majumdar@nasa.gov (A. Majumdar).

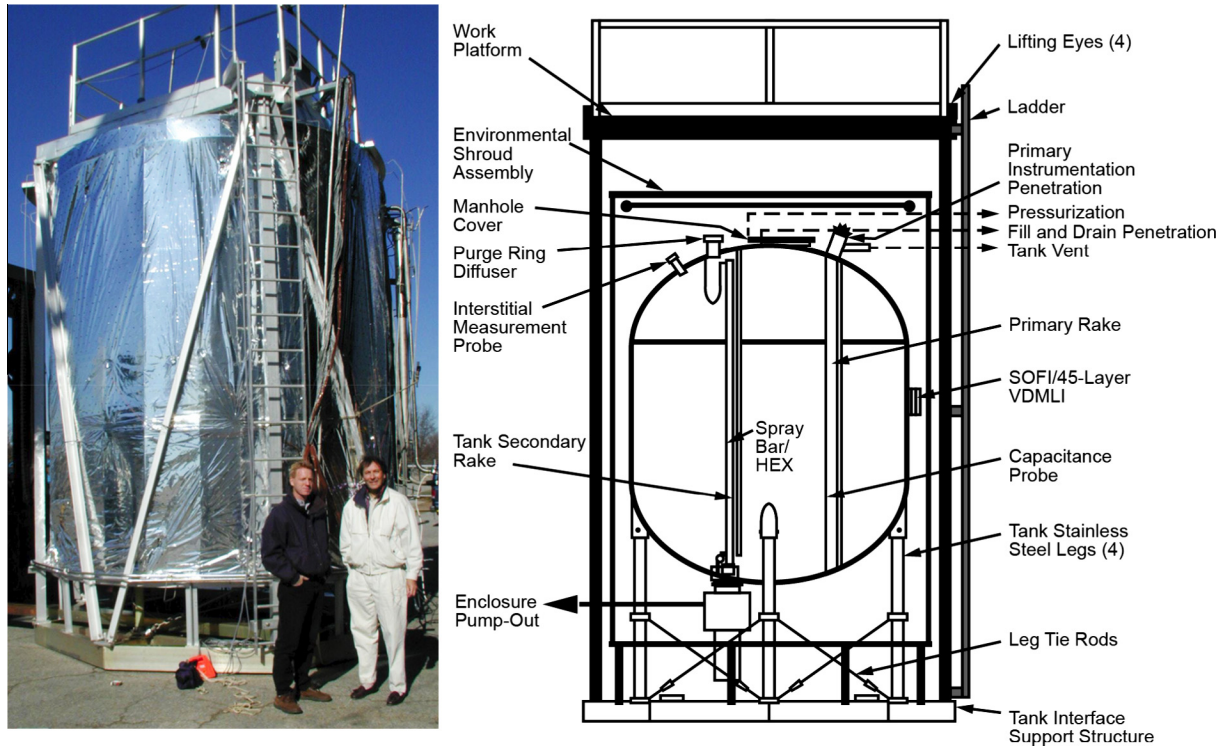


Fig. 1. Multipurpose hydrogen test bed.

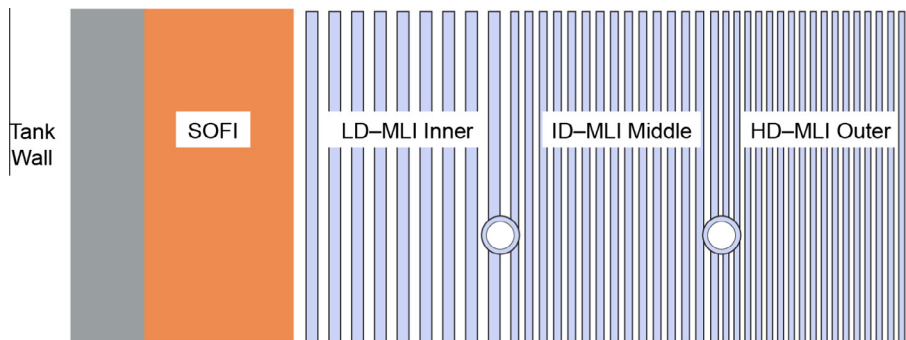


Fig. 2. Cross section of SOFI variable density MLI configuration; LD – low density, ID – intermediate density, and HD – high density.

the tank. In total, there are three sub-blankets of 10, 15, and 20 layers with a layer density of 8 layers/cm, 12 layers/cm, and 16 layers/cm, respectively (Fig. 2).

The active pressure control system used in the MHTB is a spray bar heat exchanger (HEX) thermodynamic vent system (TVS) concept shown in Fig. 3. It consists of a liquid hydrogen (LH_2) pump, Joule–Thompson (J–T) device, concentric HEX, and longitudinal spray bar system.

During the ullage mixing mode, liquid is extracted from the bottom of the tank and fed to the longitudinal HEX via the liquid pump. The fluid is then expelled radially throughout the spray bar to both the ullage and liquid. If the passive thermal protection is sufficient, then the ullage mixing mode is enough to control tank ullage pressures with no propellant loss. When mixing alone cannot control tank pressure, during the TVS operation, a small portion of liquid is fed through the J–T device, expanding the liquid and thus lowering its pressure and temperature. The expanded fluid is then passed through the HEX to condition the mixing fluid portion of the HEX loop and expelled through a pressure control orifice to space [3].

Previous attempts to model the MHTB during 1 g self-pressurization and TVS modes have been made in the past using a single node for each component of the system. The Tank System Integrated Model (TankSIM) is a Fortran-based program used to predict the behavior of cryogenic propellant under different conditions: self-pressurization, boiloff, ullage venting, mixing, and TVS (axial jet and spray bar), and two-phase HEXs [4]. TankSIM consists of eight single nodes interacting with each other:

- (1) Ullage tank wall-dome section of tank.
- (2) Ullage tank wall-cylinder section.
- (3) Bulk liquid tank wall.
- (4) Bulk liquid.
- (5) Environment.
- (6) Ullage–liquid interface.
- (7) Ullage.
- (8) Tank wall liquid–liquid film on the ullage tank walls.

Although TankSIM can predict thermodynamic performance inside a cryogenic tank with reasonable accuracy, a multinode

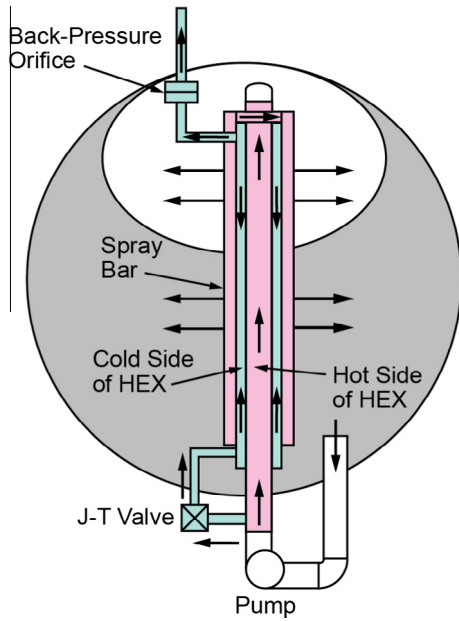


Fig. 3. Thermodynamic vent system.

Table 1
Mathematical closure.

Unknown variables	Available equations to solve
Pressure	Mass conservation equation
Flowrate	Momentum conservation equation
Fluid temperature	Energy conservation equation of fluid
Solid temperature	Energy conservation equation of solid
Fluid mass (unsteady flow)	Thermodynamic equation of state

model is needed to attain better fidelity regarding tank stratification and ullage mixing in a pressure-controlled scenario and accurately depict heat load distribution around tank structures and the tank surface area. Therefore, a multinode ullage model was developed and compared with the MHTB test data.

This paper demonstrates the simulation of 1 g self-pressurization of an LH₂ tank and the pressure control with the TVS using the multinode model. The simulation was performed with the general-purpose flow network software, GFSSP [2], developed at NASA Marshall Space Flight Center (MSFC). A coupled model of self-pressurization and TVS was developed. The purpose of the GFSSP model is to simulate the initial self-pressurization when ullage pressure rises from the initial tank pressure to the

upper bound pressure when the spray starts. Once the spray starts, a separate GFSSP model of the TVS was run in parallel with the Self-Pressurization model to provide the necessary spray input such as flowrate and temperature of the spray. The TVS model receives a boundary condition of LH₂ pressure and temperature and ullage pressure from the Self-Pressurization model. The GFSSP model results were then compared with the test data. A 50% fill level case was modeled to simulate the self-pressurization and TVS pressure cycling test.

2. Mathematical formulation and computer program

GFSSP is a finite volume-based network flow analysis program for analyzing thermofluid systems. A fluid network consists of boundary nodes, internal nodes, and branches to represent a fluid system. Boundary and internal nodes are connected through branches in series or parallel arrangements. At boundary nodes, pressures and temperatures are specified. Mass and energy conservation equations are solved in internal nodes. Flowrates are calculated in branches. A thermal system consists of solid and ambient nodes connected with conductors. A fluid and solid node are connected with a solid to fluid conductor to model conjugate heat transfer.

The mathematical closure is described in Table 1. GFSSP uses a pressure-based scheme as pressure is computed from the mass conservation equation. The mass and momentum conservation equations and thermodynamic equation of state are solved simultaneously by the Newton–Raphson method while energy conservation equations of fluid and solid are solved separately but implicitly coupled with the other equations stated above. The conservation equations are solved in conjunction with the thermodynamic equation of state. From the computed pressure and enthalpy at the nodes, all other thermodynamic properties including density, viscosity, and thermal conductivity are evaluated from built-in thermodynamic property programs. For the saturated condition, vapor quality is calculated from liquid and vapor enthalpies at the node pressure. Density and other thermophysical properties of the liquid–vapor mixture are calculated as a function of vapor quality. Further details of the mathematical formulation and solution procedure are described in Ref. [2].

Fig. 4 describes the three major parts of the GFSSP structure. The first part is the Graphical User Interface, VTASC (Visual Thermofluid Analyzer of Systems and Components). VTASC allows users to create a flow circuit by a point-and-click paradigm, and creates the GFSSP input file after the completion of the model building process. It can also create a customized GFSSP executable by compiling and linking User Subroutines with the Solver Module of the code. Users can run GFSSP from VTASC and post-process the results in the same environment. The second major part of the program is

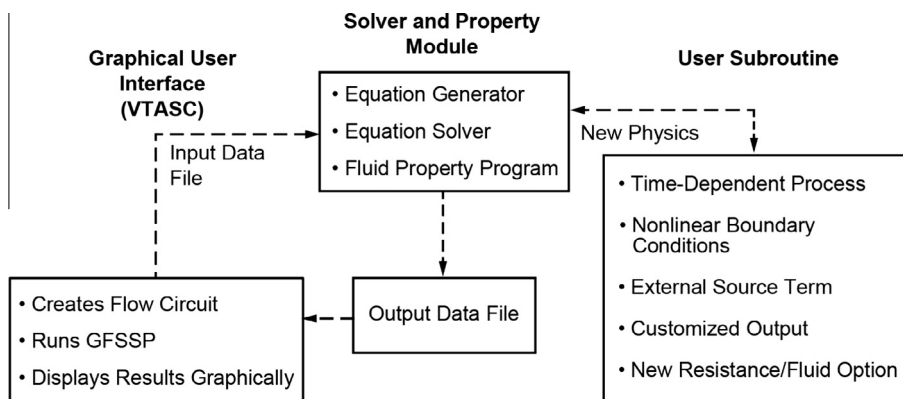


Fig. 4. GFSSP's structure showing the interaction of three major modules.

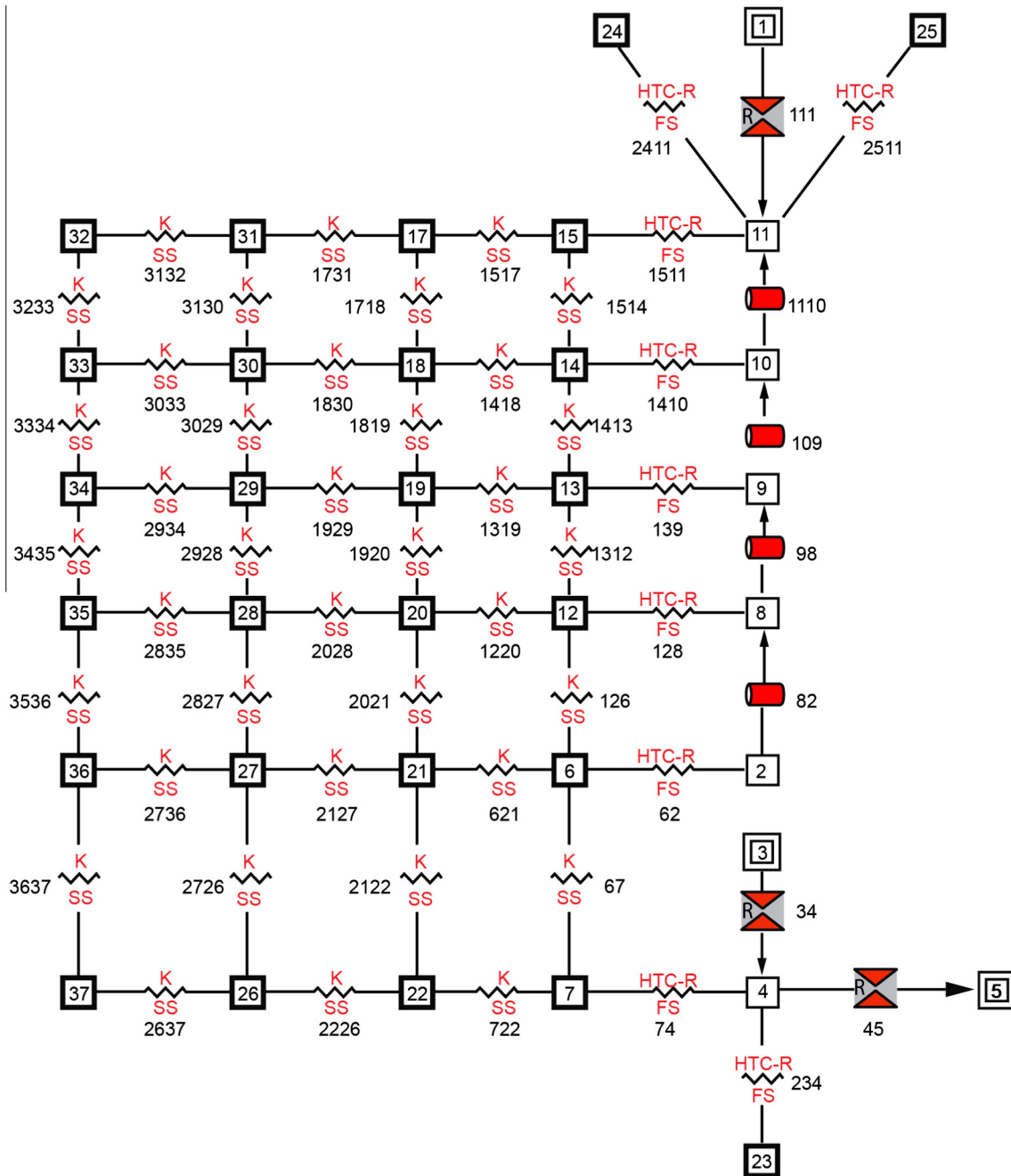


Fig. 5. GFSSP model of self-pressurization of MHTB tank.

the Solver and Property Module. This is the heart of the program that reads the input data file and generates the required conservation equations for all internal nodes and branches with the help of thermodynamic property data. It also interfaces with User Subroutines to receive any specific inputs from users. Finally, it creates output files for VTASC to read and display results. The User Subroutine is the third major part of the program, consisting of several blank subroutines that are called by the Solver Module. These subroutines allow the users to incorporate any new physical model, resistance option, fluid, etc., in the model.

2.1. Solution steps

Numerical modeling consists of the following 10 steps:

- (1) Subdivide the flow domain into fluid nodes and branches.
- (2) Subdivide the solid domain into solid nodes and conductors.
- (3) Connect the solid and fluid nodes with solid to fluid conductors.
- (4) At each fluid node, solve mass and energy conservation equations to calculate pressure and enthalpy of fluid and equation of state to compute resident mass of fluid.
- (5) At each fluid branch, solve momentum conservation equations to calculate flowrate.
- (6) From pressure and enthalpy, calculate fluid temperature and all other thermodynamic and thermophysical properties required in governing equations.
- (7) At each solid node, solve energy conservation equation to calculate temperature of the solid node.

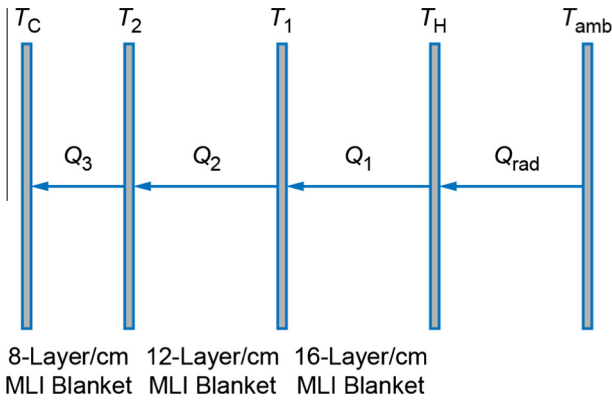


Fig. 6. MLI modeling methodology.

- (8) Steps (4)–(7) are repeated until convergence.
- (9) Steps (4)–(8) are repeated for each time step.
- (10) Terminate the calculation when final time step is reached.

3. Generalized fluid system simulation program model

The primary intent of this effort was to develop an integrated multinode model of ullage to simulate self-pressurization and pressure control by the TVS. Two separate models for self-pressurization and TVS were developed and then the models were integrated.

3.1. Self-Pressurization model

Fig. 5 shows the GFSSP model of 1g (settled) self-pressurization in the MHTB tank at the 50% fill level. Node 4 represents LH₂; nodes 2, 8, 9, 10, and 11 represent the ullage

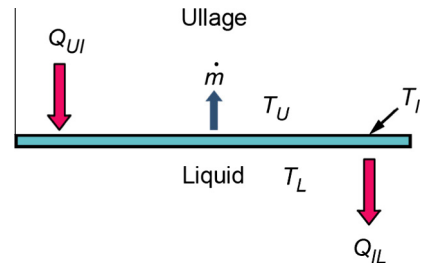


Fig. 8. Evaporative mass transfer at liquid–vapor interface.

at different fill levels (54%, 65%, 80%, 92%, and 98%). Node 3 is a pseudo-boundary node separating LH₂ from vapor hydrogen in the ullage space. The purpose of the pseudo-boundary node is to maintain a liquid–vapor interface that separates liquid and ullage in a settled condition. The pressure at the pseudo-boundary node 3 is set equal to the pressure at the ullage node 2 in the beginning of each time step. This is how the liquid node 4 is subjected to ullage pressure while maintaining liquid–vapor interface between nodes 2 and 4. Each fluid node is connected with a solid node through a solid–fluid conductor. There are four layers of solid nodes representing the Al wall and SOFI. For example, nodes 7 and 22 represent the Al wall while nodes 26 and 37 represent SOFI. MLI was wrapped around the SOFI. Modeling of heat leak through the MLI was performed in GFSSP’s User Subroutine and was applied in the outer layer of the SOFI nodes (solid nodes 32 through 37).

3.2. Modeling of heat leak through multilayer insulation

Heat transfer through the MLI can be expressed by the Modified Lockheed equation [5]:

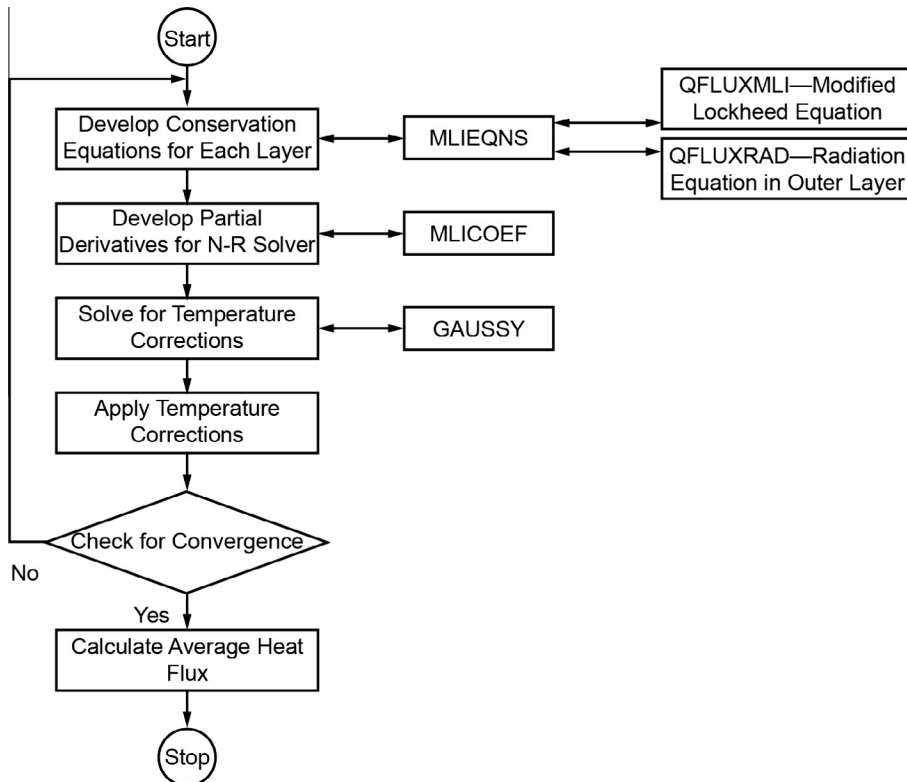


Fig. 7. Flowchart of MLI_HEAT_RATE subroutine.

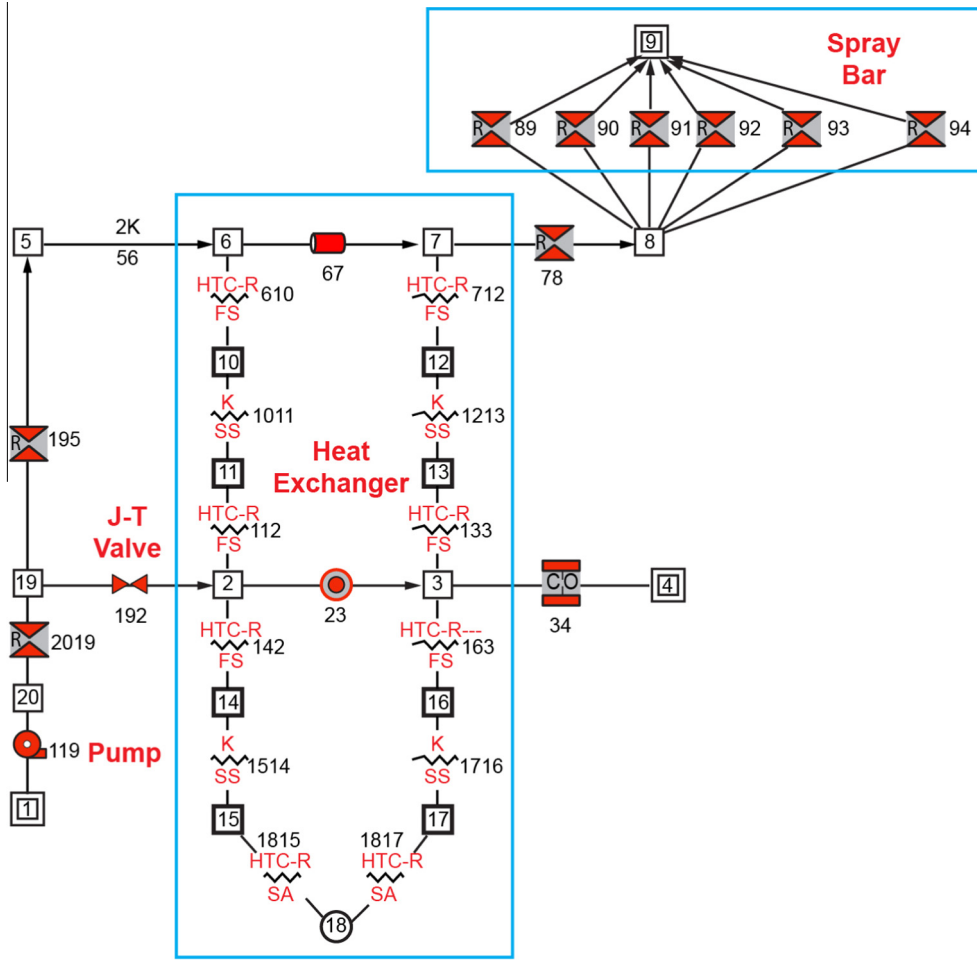


Fig. 9. GFSSP model of the TVS.

$$q = \left[\frac{C_s(0.017 + 7E - 6 * (800 - T_{avg}) + 2.28E - 2 * \ln(T_{avg})) (N_s)^{2.63} (T_h - T_c)}{N_s} + \frac{C_r \varepsilon (T_h^{4.67} - T_c^{4.67})}{N_s} + \frac{C_g P (T_h^{0.52} - T_c^{0.52})}{N_s} \right]. \quad (1)$$

The actual heat transfer, however, was calculated by introducing a degradation factor, D_f . The heat transfer rate through the MLI was expressed as:

$$q_{MLI} = D_f q, \quad (2)$$

where constants

$$\begin{aligned} C_s &= 2.4 \times 10^{-4}, \\ C_r &= 4.944 \times 10^{-10}, \\ C_g &= 14,600, \end{aligned}$$

and variables and units

q = heat flux through MLI (W/m²),
 T_{avg} = average of hot and cold boundary temperatures (K),
 N_s = MLI layer density (layers/cm),
 T_h = hot boundary temperature (K),
 T_c = cold boundary temperature (K),
 N_s = number of MLI layers,
 ε = MLI layer emissivity ($\varepsilon = 0.031$),
 P = interstitial gas pressure (torr).

Typically, several MLI blankets constitute the MLI. The mathematical modeling methodology is shown in Fig. 6. According to the law of energy conservation:

$$Q_{rad} = Q_1 = Q_2 = Q_3, \quad (3)$$

where radiative heat transfer from the shroud to the outer layer of MLI is given as:

$$q_{rad} = \frac{\sigma (T_{amb}^4 - T_{outer}^4)}{\frac{1}{\varepsilon_{MLI}} + \frac{1}{\varepsilon_{shrd}} - 1}, \quad (4)$$

where

σ = Stephan–Boltzmann constant,
 T_{amb} = temperature of inside surface of vacuum chamber (K),
 T_{outer} = temperature of outer MLI layer (K),
 ε_{shrd} = emissivity of inside surface of vacuum chamber (=0.04).

The law of energy conservation can also be expressed as:

$$Q_2(T_1, T_2) - Q_3(T_2, T_c) = 0, \quad (5)$$

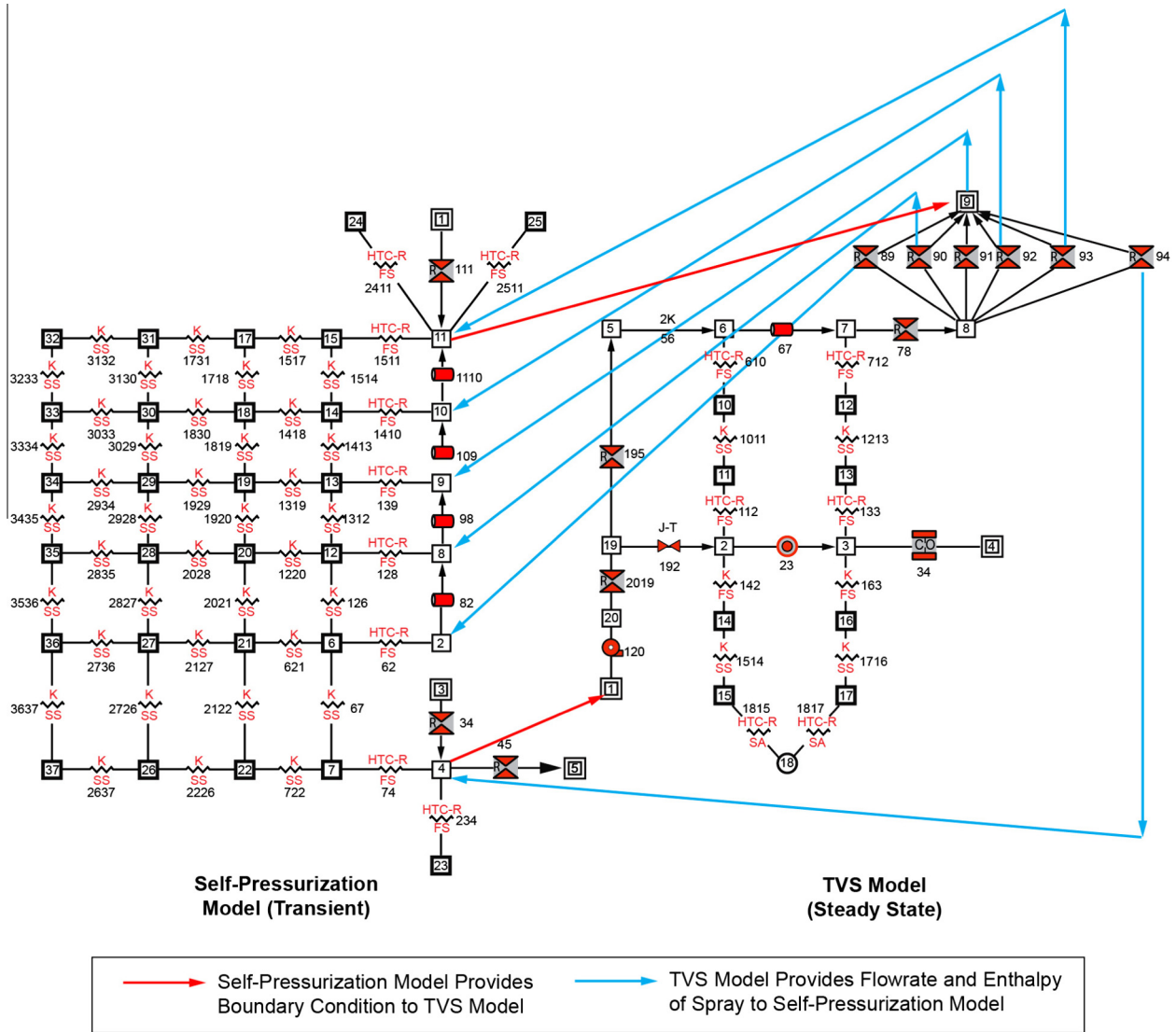


Fig. 10. Integrated Self-Pressurization and TVS models.

$$Q_1(T_H, T_1) - Q_2(T_1, T_2) = 0, \quad (6)$$

and

$$Q_{\text{rad}}(T_{\text{amb}}, T_H) - Q_1(T_H, T_1) = 0. \quad (7)$$

Eqs. (5–7) are the governing equations to calculate temperature at the outer boundary (T_H) and two intermediate temperatures (T_1 and T_2) by the Newton–Raphson method. Subroutine MLI_HEAT_RATE was developed to solve these equations. Fig. 7 shows the flowchart of the MLI_HEAT_RATE Subroutine that was called from Subroutine SORCETS. Subroutine SORCETS is called from the source code to provide any user-specified heat source to a solid node.

MLI_HEAT_RATE Subroutine calls MLIEQNS, MLICOEF, and GAUSSY to perform main computational tasks. MLIEQNS calculates residuals of the governing equations (Eqs. (5–7)). Eqs. (1) and (2) are computed in QFLUXMLI and Eq. (4) is computed in QFLUXRAD. The coefficients of the correction equation are computed in MLICOEF. The correction equations are solved in GAUSSY.

3.3. Heat transfer coefficient correlation

The heat transfer coefficient between the wall and ullage was computed from a natural convection correlation for a vertical plate [6]. The following set of equations was used for this correlation:

$$Nu = [(Nu_l)^m + (Nu_t)^m]^{1/m}, \quad m = 6, \quad (8)$$

$$Nu_t = C_t^V Ra^{1/3} / (1 + 1.4 \times 10^9 Pr / Ra), \quad (9)$$

$$Nu_l = 2 / \ln(1 + 2 / Nu^T), \quad (10)$$

$$Nu^T = \bar{C}_l Ra^{1/4}, \quad (11)$$

$$C_t^V = \frac{0.13 Pr^{0.22}}{(1 + 0.61 Pr^{0.81})^{0.42}}, \quad (12a)$$

and

$$\bar{C}_l = \frac{0.671}{[1 + (0.492 / Pr)^{9/16}]^{4/9}}, \quad (12b)$$

where $Gr = L^3 \rho^2 g \beta \Delta T / \mu^2$; $Pr = C_p \mu / k$; $Ra = Gr Pr$, and $Nu = hL/k$; subscripts t and l in Eqs. (9) and (10) refer to turbulent and laminar, respectively.

3.4. Liquid–ullage heat and mass transfer model for Self-Pressurization

Fig. 8 shows the schematic of ullage and liquid propellant where there is a heat transfer between ullage and liquid propellant that also results into evaporative mass transfer.

In this evaporative mass transfer model, a saturated layer is assumed at the interface between liquid and vapor so that $T_I = T_{\text{sat}}(P_v)$, where P_v is propellant vapor pressure in the ullage. The saturated layer receives heat from the ullage (Q_{UI}) and also rejects heat to the liquid (Q_{IL}). The difference in this heat rate contributes to the mass transfer in accordance with the law of energy conservation. The equations governing this process are as follows:

- Heat transfer from ullage to interface layer:

$$Q_{UI} = h_{UI} A (T_U - T_I) \quad (13)$$

- Heat transfer from interface to liquid:

$$Q_{IL} = h_{IL} A (T_I - T_L). \quad (14)$$

The evaporative mass transfer is expressed as

$$\dot{m} = \frac{Q_{UI} - Q_{IL}}{h_{fg}}. \quad (15)$$

h_{fg} is the enthalpy of evaporation, and the heat transfer coefficients h_{UI} and h_{IL} are computed from natural convection correlations given by:

$$h_{UI} = K_H C \frac{k_f}{L_s} Ra^n = h_{IL}, \quad (16)$$

where $K_H = 0.5$, $C = 0.27$, and $n = 0.25$.

It is assumed in this modeling that the heat transfer coefficient is the same on both sides of the liquid vapor interface. Use of liquid properties in estimating the heat transfer coefficient would result in condensation instead of evaporation. The result of such inconsistency is due to a lack of discretization in the liquid side of the interface. It may be noted that T_I represents bulk liquid temperature, not the temperature close to the interface, which should be larger than T_L . It would be more appropriate to apply boundary layer analysis to resolve this discrepancy.

3.5. Thermodynamic vent system model

The purpose of the TVS model is to estimate the temperature and flow rate of the LH₂ sprayed in the ullage to reduce the pressure and temperature. In a TVS, a small portion of LH₂ is used for cooling the ullage. Before it is sprayed, it is further cooled in a HEX where it is cooled by a cold liquid–vapor mixture produced by a J–T valve.

The GFSSP model of the TVS is shown in Fig. 9. Branch 119 represents the pump that distributes a small portion of LH₂ through the J–T valve (branch 192) and vent valve (branch 34), and the remaining portion to the spray bar consisting of six branches (branches 89, 90, 91, 92, 93, and 94). Prior to reaching the spray bar, the liquid is cooled through a HEX by rejecting some of its heat to liquid vapor mixture coming out of the J–T valve. The HEX of the GFSSP model consists of four fluid nodes (nodes 2 and 3 in the cold leg, and nodes 6 and 7 in the hot leg) and four solid nodes (nodes 10, 11, 12, and 13).

3.6. Integrated Self-Pressurization and Thermodynamic Vent System models

The integrated model is shown in Fig. 10. The integration of two models is done through an exchange of boundary conditions by writing and reading model output data from files generated while the model is running. The Self-Pressurization model on the left is the driver model. When ullage pressure reaches the maximum allowable pressure, it makes a call to run the TVS model shown on the right. Details of the integration process are shown in Fig. 11.

4. Results

This section presents the results of the combined GFSSP models of the MHTB. The transient Self-Pressurization model calls

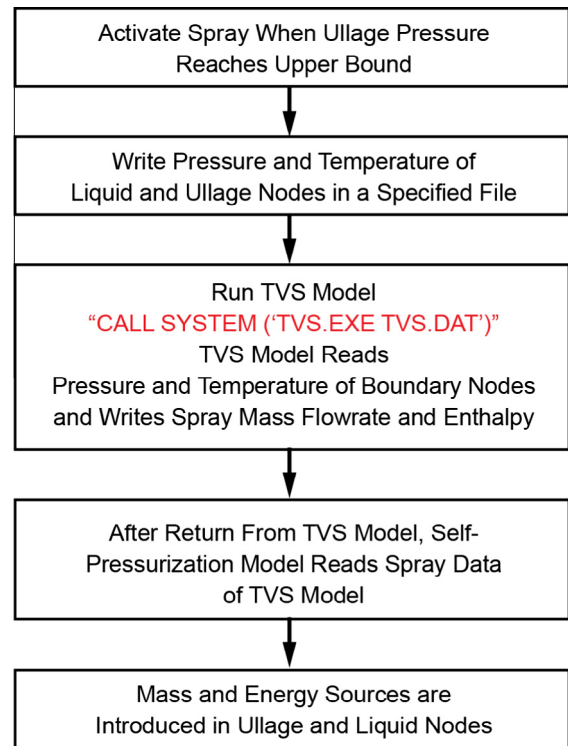


Fig. 11. The main steps of model integration.

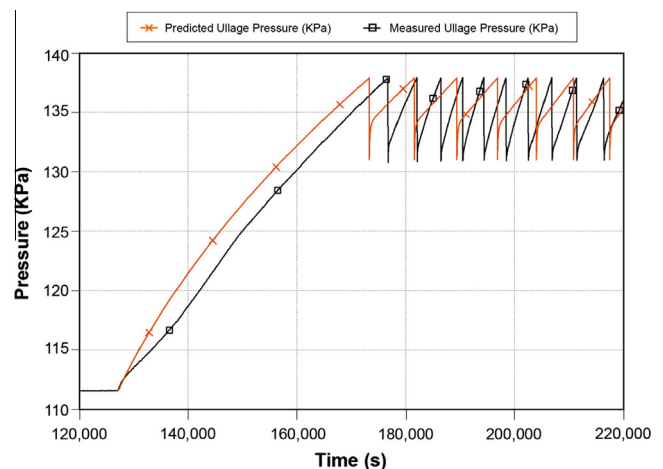


Fig. 12. Measured and predicted ullage pressure with TVS spray.

the steady-state model of the TVS whenever the TVS is operating to reduce the pressure from 138 to 131 kPa.

Fig. 12 plots the MHTB measured and predicted ullage pressure over time. The MLI degradation factor of 4 was assumed for this calculation. Several reasons for observed discrepancies include the uncertainties of heat and mass transfer coefficients at the ullage–liquid interface, and simplified modeling of spray injection and evaporation in the ullage, where liquid mass injected is uniformly distributed among the ullage nodes. Uncertainties in heat and mass transfer coefficients can be reduced by developing improved correlation of the heat transfer coefficient in the stratified ullage. Use of CFD results in the specification of spray

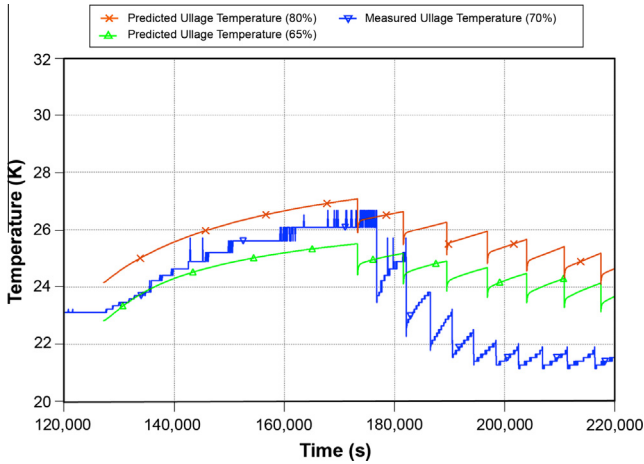


Fig. 13. Measured and predicted ullage temperature with TVS spray.

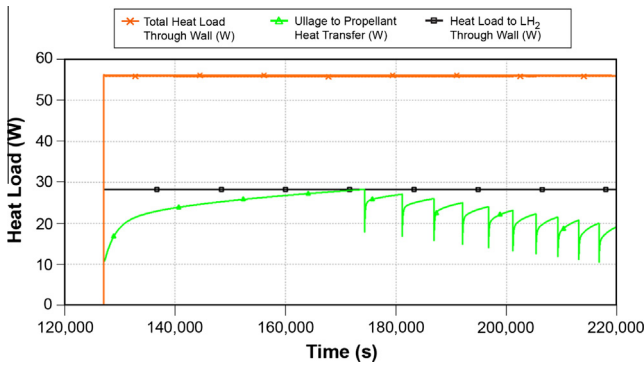


Fig. 14. Predicted heat load and ullage to propellant heat transfer.

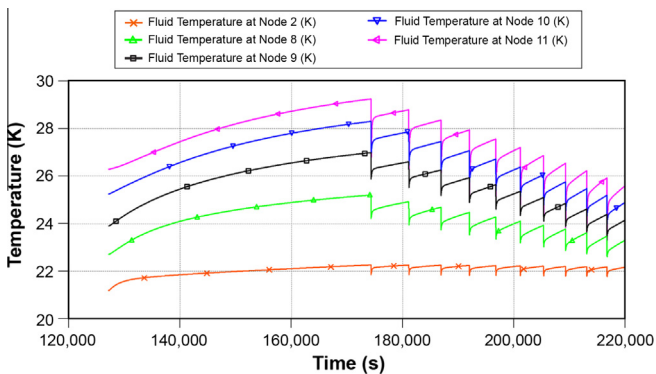


Fig. 15. Predicted ullage temperature with TVS spray history.

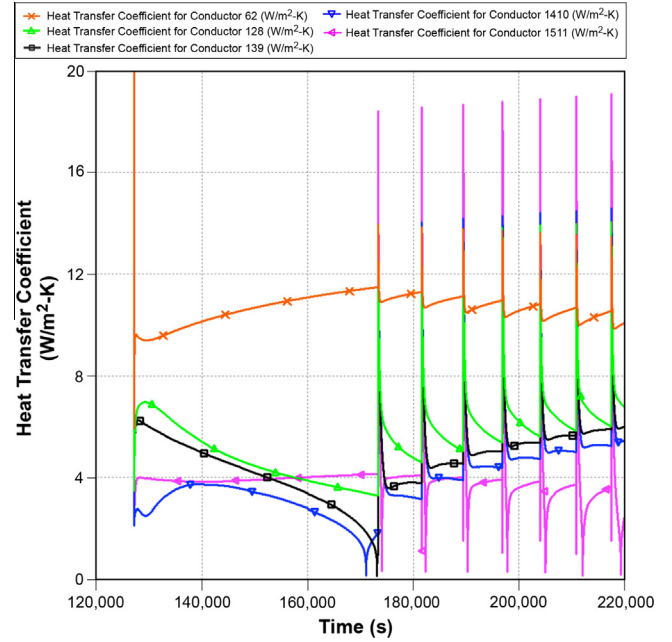


Fig. 16. Predicted heat transfer coefficients at five ullage nodes.

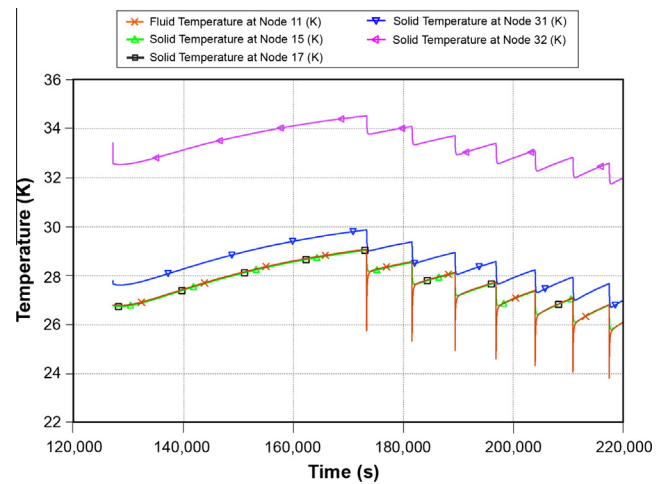


Fig. 17. Predicted radial temperature distribution at upper ullage.

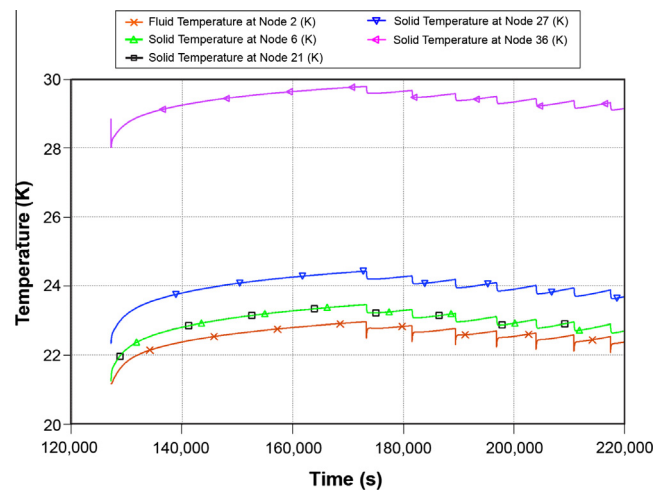


Fig. 18. Predicted radial temperature distribution at lower ullage.

distribution can also improve the accuracy of ullage temperature prediction.

Fig. 13 presents the measured ullage temperature in comparison with the predicted temperature in nodes 8 and 9 of the GFSSP model. Nodes 8 and 9 bracket the location of the temperature-sensing diode. There is good agreement in the temperature rise rate during self-pressurization. During the TVS operation, the predicted temperature is higher than the test data. This discrepancy can be attributed to the uncertainties in the prediction of flowrate and temperature of the spray.

Fig. 14 presents the predicted heat load and ullage to propellant heat transfer in watts. The predicted heat load matches closely with the test data reported in Ref. [3]. It may be noted that the heat load is evenly distributed between liquid and ullage for the 50% fill level. It is interesting to observe that ullage to liquid heat transfer is of comparable magnitude to heat leak into ullage or liquid. It may be noted that the ullage to propellant heat transfer starts dropping with the use of TVS. However, the heat load to tank remains more or less constant. The heat load to tank is primarily determined by heat transfer through the MLI. Heat transfer through the MLI is not very sensitive to ullage temperature variation.

Fig. 15 presents the predicted ullage temperature history in all five nodes located in the ullage space. Nodes 11 (pink¹) and 2 (orange) are the highest and lowest node, respectively. The drop in node temperature during TVS spray followed by the rise due to self-pressurization is observed in the temperature profile. The higher the temperature before spray is activated, the larger the temperature drop observed during spray injection. It may be noted that a future experimental program at MSFC will provide detailed temperature measurements for validation of the numerical model.

Fig. 16 presents the predicted heat transfer coefficients at the interface between the ullage and solid nodes. Conductors 62 and 1511 represent the ullage nodes closest to the liquid interface and farthest from the liquid interface (i.e., nearest to the top dome). The heat transfer coefficients are between 4 and 10 W/m² K. It is also observed that heat transfer coefficients are a strong function of density. The highest heat transfer coefficients are observed near the liquid surface (orange, Conductor 62) and lowest heat transfer coefficients occur at the highest point (green, Conductor 1511).

Figs. 17 and 18 present the radial temperature distribution (fluid to tank wall to SOFI) at the vertical locations corresponding to the ullage node nearest to top dome (Fig. 17) and the ullage node nearest the liquid interface (Fig. 18). Note that the plot does not include the temperature distribution in the MLI layers. The temperature drop through the SOFI layer is much larger than the metal wall because of low conductivity of SOFI. As noticed in Fig. 15, the temperature spike due to spray is more pronounced in the upper ullage.

The model took 8.05 h to simulate 25.8 h of real-time test with a PC laptop (Intel, 2.6 GHz). The time step was 0.1 s for self-pressurization and 0.01 s during spray.

5. Conclusions

A multinode model of self-pressurization of a cryogenic tank in ground operation has been developed using GFSSP and compared with test data. The model accounts for heat transfer through the MLI, SOFI, metal wall, and convective heat transfer between the wall and ullage/LH₂ to compute the heat load to the tank. Heat transfer through MLI and vacuumed space between the tank and shroud was calculated implicitly by solving the Modified Lockheed equation and the radiative heat flux equation during the solution of the energy conservation equation of solid nodes. It also calculates heat and mass transfer between ullage and liquid propellant. The Self-Pressurization model also includes the effect of liquid spray to cool the ullage and reduce the pressure. A TVS model was integrated with the Self-Pressurization model to provide the boundary condition of spray. The prediction of pressure cycling of the integrated model matches satisfactorily with the test data. Future modeling efforts will include the development of solution algorithm for flow separation between the liquid and gas phase to account for liquid–ullage dynamics in space under a microgravity environment.

Acknowledgements

This work was supported by the NASA Space Technology Mission Directorate's Technology Demonstration Missions Program under the Evolvable Cryogenics Project. The authors wish to thank the Scientific and Technical Information Publications Office of NASA Marshall Space Flight Center for the preparation of this manuscript.

References

- [1] Martin JJ, Hastings LJ. Large-scale liquid hydrogen testing of a variable density multilayer insulation with a foam substrate. NASA/TM-2001-211089. Huntsville (AL): NASA Marshall Space Flight Center; June 2001. 88pp.
- [2] Majumdar AK, LeClair AC, Moore R, Schallhorn PA. Generalized fluid system simulation program, Version 6.0. NASA/TM-2013-217492; October 2013. <https://gfsfp.msfc.nasa.gov/pdf/NASA_TM_2013_217492.pdf>.
- [3] Hastings LJ, Flachbart RH, Martin JJ, Hedayat A, Fazah M, Lak T, et al. Spray bar zero-gravity vent system for on-orbit liquid hydrogen storage. NASA/TM-2003-212926. Huntsville (AL): NASA Marshall Space Flight Center; October 2003. 160pp.
- [4] Bolshinskiy L, Hastings LJ, Hedayat A, et al. Tank system integrated model TankSIM Version 5.0. ESSA_FY13-01202; May 2013.
- [5] Hastings LJ, Hedayat A, Brown TM. Analytical modeling and test correlation of variable density multilayer insulation for cryogenic storage. NASA/TM-2004-213175. Huntsville (AL): NASA Marshall Space Flight Center; May 2004. 46pp.
- [6] Rohsenow WM, Hartnett JP, Cho YI. Handbook of heat transfer. 3rd ed. McGraw-Hill; 1998. p. 4.13.

¹ For interpretation of color in Figs. 15 and 16, the reader is referred to the web version of this article.